Adenomatous polyposis coli protein nucleates actin assembly and synergizes with the formin mDia1

Kyoko Okada,[1] Francesca Bartolini,[4] Alexandra M. Deaconescu,[2] James B. Moseley,[1] Zvonimir Dogic,[3] Nikolaus Grigorieff,[2] Gregg G. Gundersen,[4] and Bruce L. Goode[1]

[1]Department of Biology, [2]Howard Hughes Medical Institute and Department of Biochemistry, and [3]Department of Physics, Rosenstiel Basic Medical Sciences Research Center, Brandeis University, Waltham, MA 02454
[4]Department of Pathology and Cell Biology, Columbia University, New York, NY 10032

The tumor suppressor protein adenomatous polyposis coli (APC) regulates cell protrusion and cell migration, processes that require the coordinated regulation of actin and microtubule dynamics. APC localizes in vivo to microtubule plus ends and actin-rich cortical protrusions, and has well-documented direct effects on microtubule dynamics. However, its potential effects on actin dynamics have remained elusive. Here, we show that the C-terminal "basic" domain of APC (APC-B) potently nucleates the formation of actin filaments in vitro and stimulates actin assembly in cells. Nucleation is achieved by a mechanism involving APC-B dimerization and recruitment of multiple actin monomers. Further, APC-B nucleation activity is synergistic with its in vivo binding partner, the formin mDia1. Together, APC-B and mDia1 overcome a dual cellular barrier to actin assembly imposed by profilin and capping protein. These observations define a new function for APC and support an emerging view of collaboration between distinct actin assembly–promoting factors with complementary activities.

Introduction

Dynamic reorganization of the actin cytoskeleton is indispensable for polarized cellular processes such as cell motility and asymmetric cell division. The de novo formation of actin filaments is a crucial step in these events. As such, cells require a variety of actin nucleators that are harnessed to the assembly of different actin structures (Chesarone and Goode, 2009). Further, the proper formation of actin structures underlying cell motility, cell polarization, and cytokinesis depends on closely coordinated interplay between the actin and microtubule cytoskeletons (Drubin and Nelson, 1996; Li and Gundersen, 2008).

Adenomatous polyposis coli (APC), a large 350-kD multidomain protein (Fig. 1 A), is a tumor suppressor linked to colorectal cancer and has an established role in regulating microtubule cytoskeleton organization and dynamics (McCartney and Näthke, 2008). In addition, APC has been suggested to influence actin cytoskeleton regulation, but the underlying mechanism has been unclear. Previous studies have shown that the C-terminal "Basic" region of APC (Fig. 1 A) binds to microtubules and stabilizes microtubules in cells together with its binding partner EB1 (Munemitsu et al., 1994; Su et al., 1995; Kita et al., 2006). Loss of the C terminus of APC also causes defects in directional cell migration, a process that requires close coordination between the microtubule and actin cytoskeletons (Oshima et al., 1997). To date, the possible direct effects of APC on actin dynamics have not been well explored, and it has been postulated that the primary influence of APC on actin cytoskeleton remodeling occurs through indirect mechanisms, mediated by APC interactions with its binding partners, including its N-terminal associations with IQGAP and ASEF (Kawasaki et al., 2000; Watanabe et al., 2004) and its C-terminal associations with the formin mDia (Wen et al., 2004). However, recently it was shown that the C-terminal Basic domain of APC binds directly to F-actin (Moseley et al., 2007).

Here, we demonstrate that the APC-Basic domain induces actin assembly in vivo and potently nucleates actin polymerization in vitro, providing a direct mechanism for APC in regulating actin-based cell protrusion, motility, and polarity.

Correspondence to Bruce L. Goode: goode@brandeis.edu

Abbreviations used in this paper: APC, adenomatous polyposis coli; TIRF, total internal reflection fluorescence.

The Rockefeller University Press $30.00
J. Cell Biol. Vol. 189 No. 7 1087–1096
www.jcb.org/cgi/doi/10.1083/jcb.201001016

Results and discussion

APC stimulates actin assembly in vivo and in vitro

To investigate effects of the C-terminal Basic (B) region of APC on cellular actin dynamics, we introduced a plasmid for expression of GFP-APC-B into serum-starved NIH3T3 cells by microinjection (Fig. 1 B). GFP-APC-B induced formation of bright-staining F-actin structures, and colocalized with them (Fig. 1 B). Quantification of the effects showed that GFP-APC-B caused a ∼40% increase in total cellular F-actin content compared with cells injected with empty vector (Fig. 1 C). Further, when adjacent cells were microinjected, we observed a marked accumulation of F-actin at cell–cell contacts (Fig. 1 B, linescan). These observations suggested that APC-B might directly or indirectly induce actin filament assembly.

To investigate the mechanistic basis of these observations, we purified APC-B and a longer polypeptide (APC-C; Fig. 1 A) and tested their effects on actin assembly in vitro. Both polypeptides accelerated actin assembly in a concentration-dependent manner, with potent effects at low nanomolar concentrations (Fig. 1 D, APC-C; Fig. S2 A). Electron microscopy and total internal reflection fluorescence (TIRF) microscopy analysis of samples from early time points in the reactions showed that APC-B and APC-C induce formation of unbranched filaments (Fig. 1, E and F). APC-B did not sever filaments to promote disassembly (Fig. 1 G) or cap the growing barbed ends (Fig. 1 I) of preformed filaments to inhibit growth, demonstrating that the ability of APC-B to promote actin assembly does not stem from severing or capping. Further, APC-B–induced actin assembly was blocked by the barbed end-capping agent cytochalasin D (Fig. 1 H). Together, these data show that APC-B promotes robust de novo formation of actin filaments that grow primarily from their barbed ends.

Next, we directly compared the nucleation activities of APC-B and the FH1-FH2 domain-containing C-terminal half of mouse formin mDia1 (C-mDia1) at different actin concentrations (Fig. 2 A). Interestingly, APC-B was a more effective nucleator than C-mDia1 at low actin concentrations, which could be an important property in vivo under conditions where free actin monomers are limiting. Although formin-induced actin nucleation was partially suppressed in the presence of profilin, APC-B–induced nucleation was not (Fig. 2, B and C). Analysis of filament barbed end elongation rates in the presence of profilin by TIRF microscopy further revealed that, unlike formins, APC-B did not accelerate elongation (Fig. 2 D and Videos 1–3). These results are consistent with APC lacking recognizable profilin-binding motifs (Fig. S1), and highlight some of the major differences between APC-B and formins as actin assembly-promoting factors.

APC mechanism of actin nucleation

All nucleators identified to date use one of three mechanisms to promote de novo formation of actin filaments (Chesarone and Goode, 2009). Arp2/3 complex is proposed to structurally mimic the barbed end of an actin filament (Kelleher et al., 1995). Formins appear to stabilize spontaneously formed polymerization intermediates, actin dimers and trimers (Pring et al., 2003). Spire, Cobl, Lmod, and JMY contain WH2 domains and recruit actin monomers to form prenucleation complexes that "seed" polymerization (Quinlan et al., 2005; Ahuja et al., 2007; Chereau et al., 2008; Zuchero et al., 2009). Our data above suggest that APC-B uses a mechanism distinct from Arp2/3 complex because APC-B promotes unbranched nucleation, and distinct from formins because APC-B does not protect barbed end growth from capping proteins or accelerate elongation. Therefore, we explored whether APC-B recruits actin monomers.

In native PAGE assays, G-actin alone migrated toward the anode, whereas APC-B alone migrated toward the cathode consistent with its high content of basic residues (pI = 10.4; Fig. 2 E). In the presence of APC-B, G-actin migration was reversed, comigrating with APC-B toward the cathode and increasing the density of the gel band (Fig. 2 E, bottom). Reactions contained 100 mM KCl, as well as latrunculin B, which blocks actin polymerization. These data suggest that APC-B physically associates with G-actin. Second, we tested APC-B–actin interactions by sedimentation velocity analysis in the presence of latrunculin B. Both APC-B and G-actin migration patterns shifted when mixed together compared with the migration patterns of each protein alone (Fig. S2, B and C), providing further support for their association. Third, we tested APC-B binding to actin monomers based on its ability to increase the fluorescence signal of pyrene-labeled G-actin (0.1 µM) under nonpolymerizing conditions including the presence of latrunculin B (Fig. 2 F). Binding was concentration dependent and saturated almost precisely at a 1:2 molar ratio of APC-B to G-actin (Fig. 2 F, dotted line) and with an apparent dissociation constant of 17.3 nM. Further addition of 5 µM profilin did not alter the effects of 50 nM APC-B on the fluorescence of 100 nM pyrene–G-actin (Fig. 2 G). This suggests that either APC-B and profilin have nonoverlapping binding sites on G-actin or APC-B very efficiently outcompetes profilin for G-actin binding, explaining why APC-B nucleation activity is not suppressed by the presence of profilin.

To further dissect the nucleation activity of APC, we generated a series of N- and C-terminally truncated APC-B polypeptides and compared their abilities to stimulate actin assembly and to bind G-actin (Fig. 3 A; Fig. S3, A–C). This analysis identified two sequences in APC-B that are critical for nucleation in vitro, ANS1 (residues 2326–2353) and ANS2 (residues 2526–2612). Moreover, constructs ΔN4 and ΔN5, which both delete ANS1, drastically reduced APC-B–induced actin assembly in vivo (Fig. 3, B and C), suggesting that the ability of APC-B to promote actin assembly in vivo stems from its nucleation activity. Importantly, the truncations did not significantly alter the net charge of the APC-B polypeptides (listed in Fig. 3 A), indicating that nucleation effects are not due to nonspecific electrostatic attractions between APC-B and actin. The specificity of the nucleation effects was further demonstrated by the observation that ANS2 is not required for APC-B binding to microtubules (Fig. 3 A and Fig. S3 D).

We next tested the importance of ANS1 and ANS2 for APC-B binding to G-actin by comparing the effects of APC-B, ΔN4, and ΔC2 in both the pyrene-actin fluorescence and native PAGE assays. In both assays, ANS1 was critical for APC-B

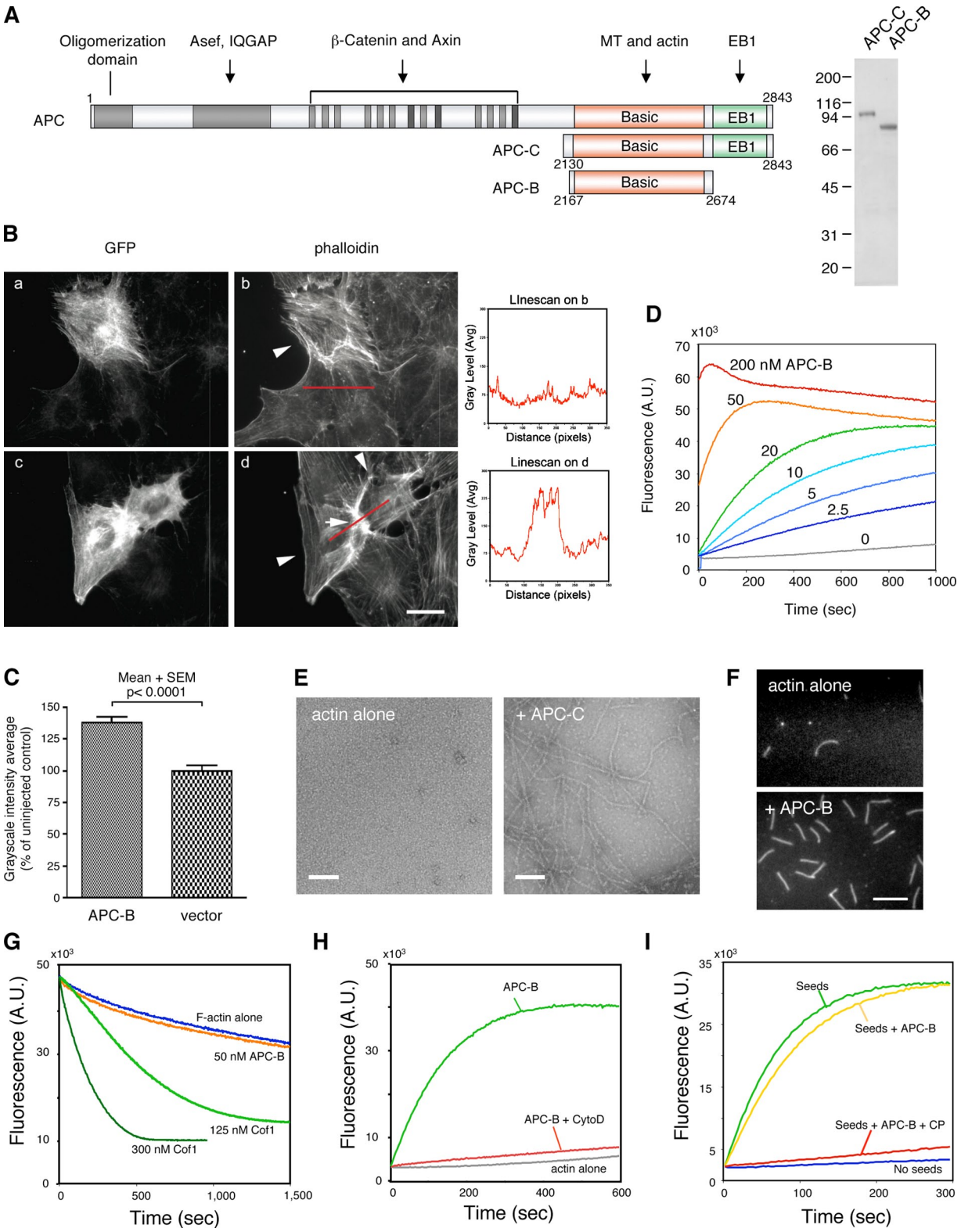

Figure 1. **APC directly nucleates actin assembly.** (A) Schematic of APC, and Coomassie-stained gel of purified APC polypeptides. (B) GFP fluorescence and rhodamine-phalloidin staining of serum-starved NIH3T3 cells. Arrowheads, cells microinjected with EGFP-APC-B plasmid. Arrow, F-actin accumulation at cell–cell junction. Bar, 10 μm. Right panel shows linescan quantification of F-actin at cell–cell junctions in the absence (b, red line) or presence (d, red line) of GFP-APC-B. (C) Quantification of F-actin levels in cells ($n > 50$ cells). (D) Assembly of actin (2 μM; 5% pyrene labeled) induced by 0–200 nM APC-B. (E) Electron micrographs of actin polymerized for 30 s in the presence or absence of 50 nM APC-C. Bar, 100 nm. (F) TIRF microscopy of actin (1 μM; 30% labeled) assembled in the presence and absence of 2 nM APC-B, visualized 2–3 min after initiation of polymerization. Bar, 5 μm. (G) Severing and depolymerization of 2 μM preformed actin filaments was induced by Cof1 but not APC-B upon addition of 3 μM Vitamin-D binding protein (a monomer sequestering factor) to induce depolymerization. (H) 100 nM cytochalasin D blocks the assembly of actin (2 μM) stimulated by 20 nM APC-B. (I) APC-B does not protect filament barbed ends against 100 nM CapZ (CP) in seeded filament elongation assay.

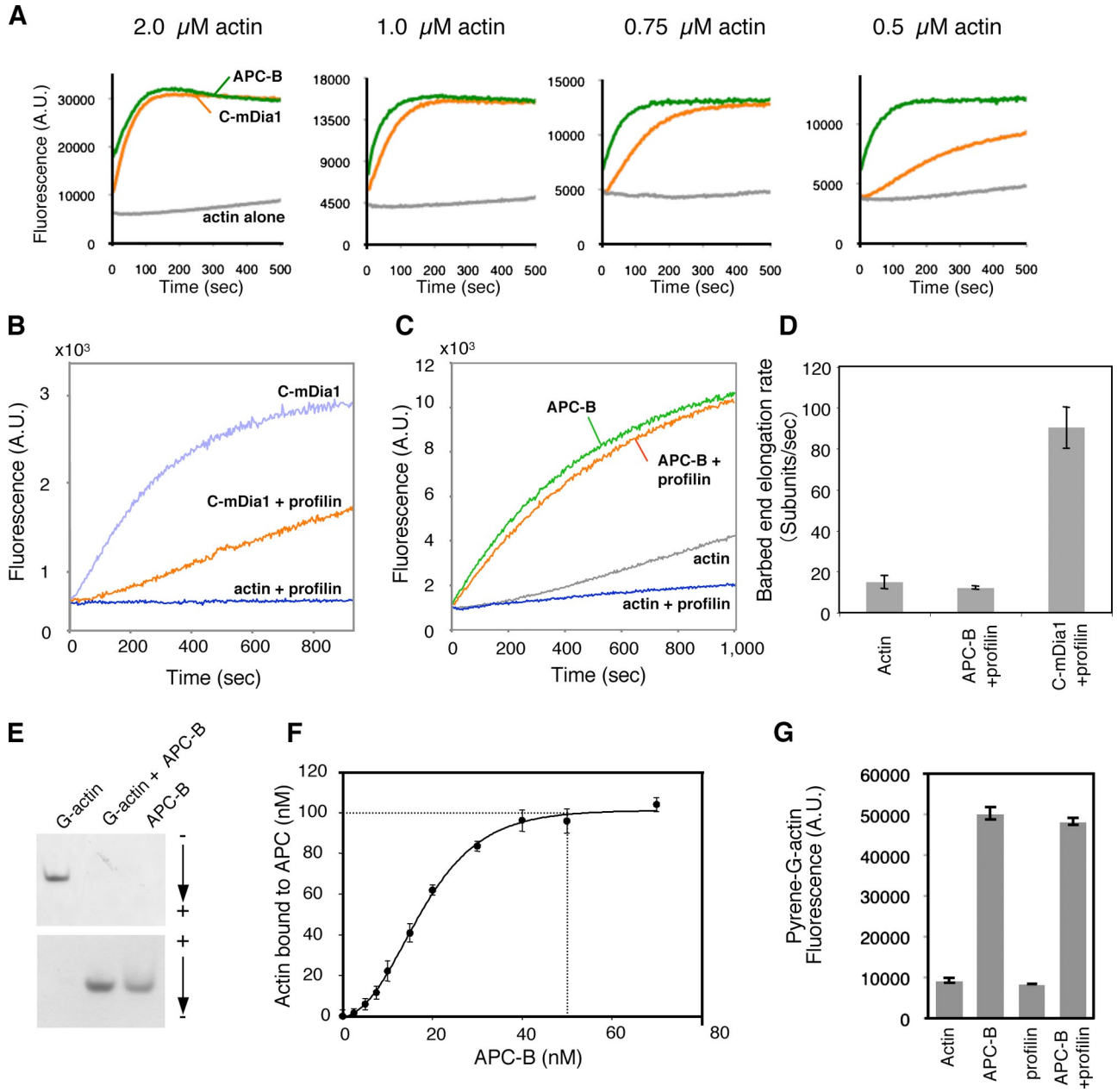

Figure 2. **Properties of APC as an actin assembly–promoting factor.** (A) Comparison of nucleation effects for 20 nM APC-B and 20 nM C-mDia1 at different concentrations of actin monomers (5% pyrene labeled). (B and C) Effects of 2 nM C-mDia1 or 20 nM APC-B on the assembly of actin (2 μM; 5% pyrene labeled) in the presence or absence of 3 μM profilin. (D) Increase in barbed end elongation rate of individual actin filaments by C-mDia1 and profilin but not by APC-B. Rates of elongation were measured in real time by TIRF microscopy and averaged for >10 filaments. Error bars, standard deviation. (E) Native PAGE assay for APC-B binding to G-actin. Reactions were loaded on gels and run toward either the cathode (top) or anode (bottom), then gels were Coomassie stained. (F) Fluorescence-based assay for concentration-dependent binding of APC-B (0–75 nM) to G-actin (100 nM; 100% pyrene labeled). Dashed line indicates binding saturation at a 1:2 molar ratio of APC-B to actin. Error bars, standard deviation (n = 3). (G) 5 μM profilin does not affect the ability of 50 nM APC-B to increase the fluorescence of pyrene–G-actin (0.1 μM, 100% labeled). Error bars, standard deviation (n = 3).

binding to G-actin (Fig. S3, B, C, and E). On the other hand, deletion of ANS2 had no effect on APC-B binding to G-actin in pyrene fluorescence assays, yet disrupted formation of stable APC-B–actin complexes in native PAGE assays. Importantly, ΔC2 (which lacks ANS2) had the same 2:1 stoichiometry of APC-B–actin binding. These data suggest that ANS1 is crucial for actin binding, whereas ANS2 makes a distinct mechanistic contribution to formation of stable APC-B–actin complexes (see dimerization evidence below).

One major class of actin nucleators, which includes Spire, Cobl, Lmod, and JMY, contains tandem actin monomer-binding domains (typically WH2 domains) used to recruit up to four actin monomers into prenucleation complexes (Quinlan et al., 2005; Ahuja et al., 2007; Chereau et al., 2008; Zuchero et al., 2009). In Spire and Cobl, two WH2 domains are sufficient for weak nucleation, but all four are required for strong activity. Our stoichiometry data indicate that each APC-B molecule binds two actin monomers (Fig. 2 F). This prompted us to test

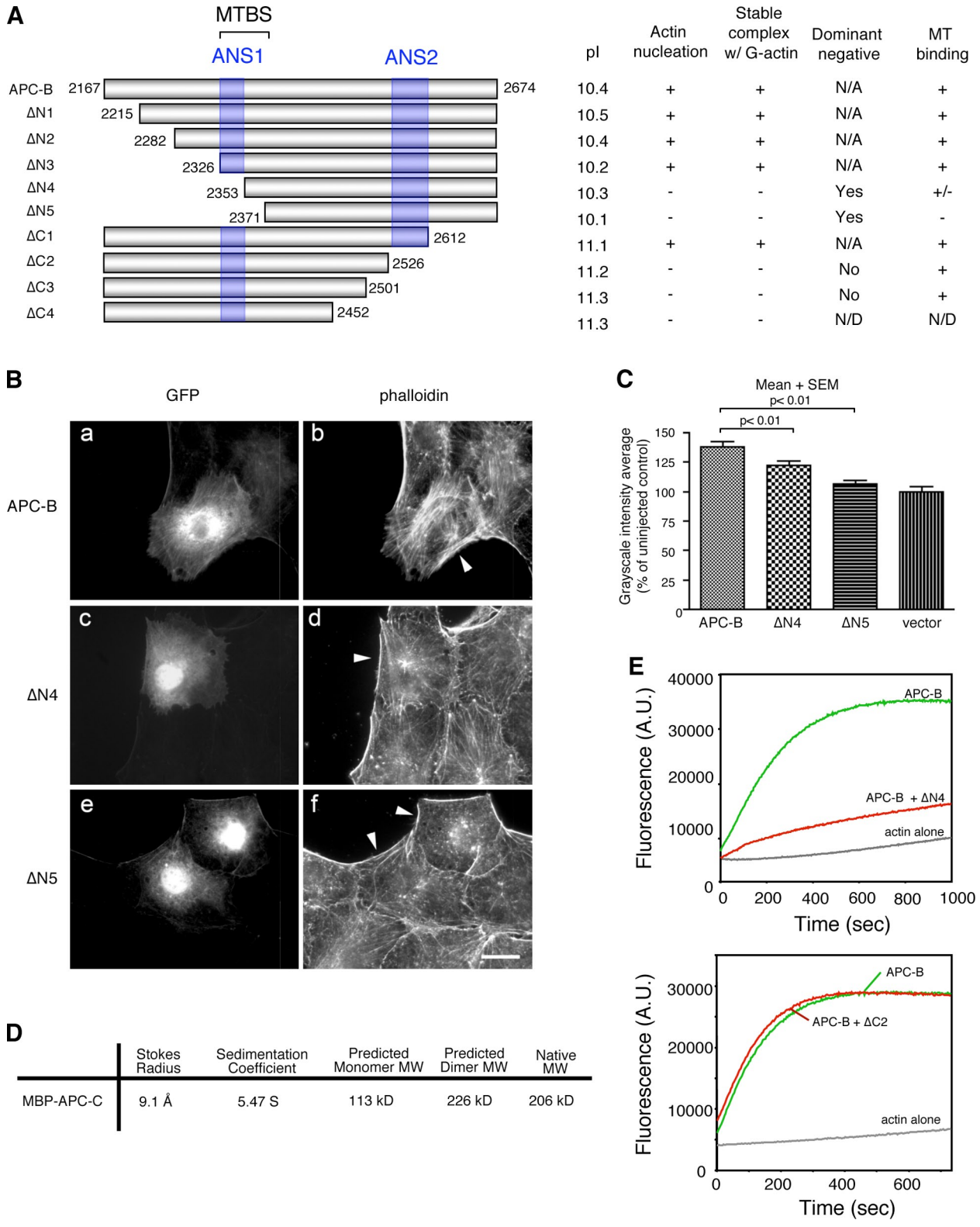

Figure 3. **Dissection of APC-B actin nucleation activity and mechanism.** (A) Schematic of APC-B truncated polypeptides analyzed. The actin nucleation sequences identified (ANS1 and ANS2) are shaded blue. MTBS, microtubule binding site; N/A, not applicable; N/D, not determined. (B) Deletion of ANS1 diminishes the actin nucleation activity of APC-B in cells. Serum-starved NIH3T3 cells microinjected with EGFP-APC-B, EGFP-APC-B-ΔN4, or EGFP-APC-B-ΔN5 plasmids (arrows) were fixed and imaged for GFP fluorescence and rhodamine-phalloidin staining. Bar, 10 μm. (C) Quantification of total cellular F-actin levels ($n > 50$ cells). (D) Dimerization of APC-C polypeptide. Stokes radius and sedimentation coefficient were determined for MBP–APC-C and used to calculate its native molecular weight (MW). Predicted MW of monomer and dimer for MBP–APC-C are listed for comparison. (E) Dominant-negative effects of truncated APC-B polypeptides on wild-type APC-B–induced actin assembly. Reactions contain actin (2 μM; 5% pyrene labeled) and 50 nM wild-type APC-B, with or without 50 nM APC-B–ΔN4 (top) or 50 nM APC-B–ΔC2 (bottom).

whether APC-B might dimerize to increase its actin-recruiting capacity. Previous studies have shown that the N terminus of APC dimerizes (Joslyn et al., 1993), but the properties of the C terminus have remained uncharacterized. Therefore, we determined the Stokes radii and sedimentation coefficients for APC-C and from these data calculated its native MW (Fig. 3 D), which suggested that APC-C forms a stable and extended dimer. A similar hydrodynamic analysis of truncation mutants showed that loss of ANS1 (ΔN4) did not affect dimerization (multimerization state of 1.97), whereas loss of ANS2 (ΔC2) weakened dimerization (multimerization state of 1.49). Further, ΔN4 dominantly interfered with the actin nucleation activity of wild-type APC-B, whereas ΔC2 did not (Fig. 3 E). The simplest interpretation of these results is that ΔN4, which fails to bind actin, may interact with wild-type APC-B to form nucleation-incompetent heterodimers, whereas ΔC2 is dimerization impaired and therefore does not interfere with wild-type APC-B activity. Given the 2:1 binding stoichiometry of actin to APC-B, we propose that each APC-B dimer can recruit up to four actin monomers in a prenucleation complex.

Synergy between APC-B and mDia1 in assembling actin filaments

We next explored the functional relationship of APC-B and mDia1 in actin assembly. As mentioned above, APC-B nucleates actin assembly efficiently in the presence of profilin, whereas C-mDia1 does not (Fig. 2, B and C). On the other hand, C-mDia1 protects growing barbed ends of filaments from capping proteins, whereas APC-B does not (Fig. 1 H). Given these complementary activities, and their reported physical interactions (Wen et al., 2004), we tested the combined effects of APC-B and C-mDia1 on actin assembly in the presence of profilin and capping protein, which presents a double barrier to actin assembly reflective of in vivo conditions (Fig. 4 A). APC-B alone and C-mDia1 alone showed only a weak ability to stimulate actin assembly under these conditions. However, combining the two proteins yielded strong synergistic effects. Together, APC-B and C-mDia1 produced a 3.6-fold higher actin assembly activity than the sum of their individual effects (Fig. 4 B). Consistent with these biochemical data, the ability of APC-B to induce actin assembly in NIH3T3 cells was greatly reduced after silencing of mDia1 expression by siRNA oligos but not control silencing of GAPDH (Fig. 4, C and D). Importantly, F-actin fluorescence intensities in cells did not differ significantly for mDia1 and GAPDH silencing alone (no APC injection). Together, these results show that APC-B and mDia1 can synergize to stimulate actin assembly both in a purified system and in living cells.

Based on these data, we propose the following model for APC-B/mDia1 synergy in assembling actin filaments (Fig. 4 E). APC-B dimers recruit up to four actin monomers to form a polymerization seed. This occurs efficiently in the presence of profilin. Next, mDia1 captures the barbed end of the nascent seed and moves processively with the growing end, accelerating elongation through FH1–profilin–actin interactions (Kovar and Pollard, 2004; Romero et al., 2004) while shielding growing ends from capping protein (Zigmond et al., 2003; Moseley et al., 2004).

Conclusions

Including APC, seven bona fide actin nucleators have now been identified, each with unique properties and mechanisms. The properties of APC-B as a nucleator are that it: (1) assembles unbranched filaments; (2) does not require a cofactor, whereas Arp2/3 complex does; (3) dimerizes and requires two functional halves (separate molecules) for nucleation; (4) fails to protect barbed ends of filaments from capping protein; (5) nucleates efficiently from profilin–actin; and (6) nucleates by recruiting up to four actin monomers, but does not contain recognizable WH2 sequences. Thus, APC appears to share at least some properties with nucleators of the Spir/Cobl/Lmod/JMY class, but also exhibits unique properties (most notably, it dimerizes and has no WH2 domains), suggesting that overall it has a novel mechanism of nucleation.

Because APC is well established as a microtubule regulator and binds to microtubules via its Basic region (Munemitsu et al., 1994), it was interesting to learn that the Basic region also nucleates actin assembly. Our truncation analysis showed that ANS2 is required for actin nucleation, and possibly dimerization, but not for microtubule binding (Fig. S3 D). Our data also indicate a close proximity and partial overlap of the microtubule-binding region of APC-B with ANS1; thus, steric hindrance could explain why APC-B interactions with actin and microtubules are mutually exclusive (Moseley et al., 2007). In addition, these observations raise the question of how APC interactions with actin and microtubules are differentially regulated in vivo and/or constrained to specific cellular compartments. This could involve post-translational modifications of APC and/or specific binding partners.

Our data also point to a strong synergy between APC-B and mDia1 in promoting actin assembly in the combined presence of profilin and capping protein in vitro and in cells (Fig. 4). This offers a functional explanation for the interactions between APC and mDia (Wen et al., 2004), although in the absence of more detailed information about their association, it is unclear whether synergy requires direct APC–mDia interactions. Nonetheless, this highlights how cells may combine two different actin assembly–promoting factors with unique strengths to bypass common inhibitors of nucleation and elongation. This synergy between APC-B and mDia1 could occur in vivo at actin-rich zones of membrane protrusion and cell–cell contact, where both APC and mDia1 have been localized (Watanabe et al., 1997; Rosin-Arbesfeld et al., 2001; Carramusa et al., 2007). Such a mechanism would offer increased spatiotemporal control over actin assembly in vivo, restricting new growth to locations where two separate factors had been successfully recruited and activated. This strategy may also extend to other pairs of actin assembly–promoting factors that have been shown to physically interact (e.g., Spire and formins, JMY, and Arp2/3 complex), and for which mounting genetic and biochemical evidence supports functional synergy (Bosch et al., 2007; Quinlan et al., 2007; Zuchero et al., 2009).

Finally, our results may have possible implications for how truncations in APC lead to colorectal tumor formation. Cancer-causing mutations in APC delete the entire C terminus, including the Basic domain. This stabilizes β-catenin, which is sufficient to induce tumor formation, but it has also been suggested

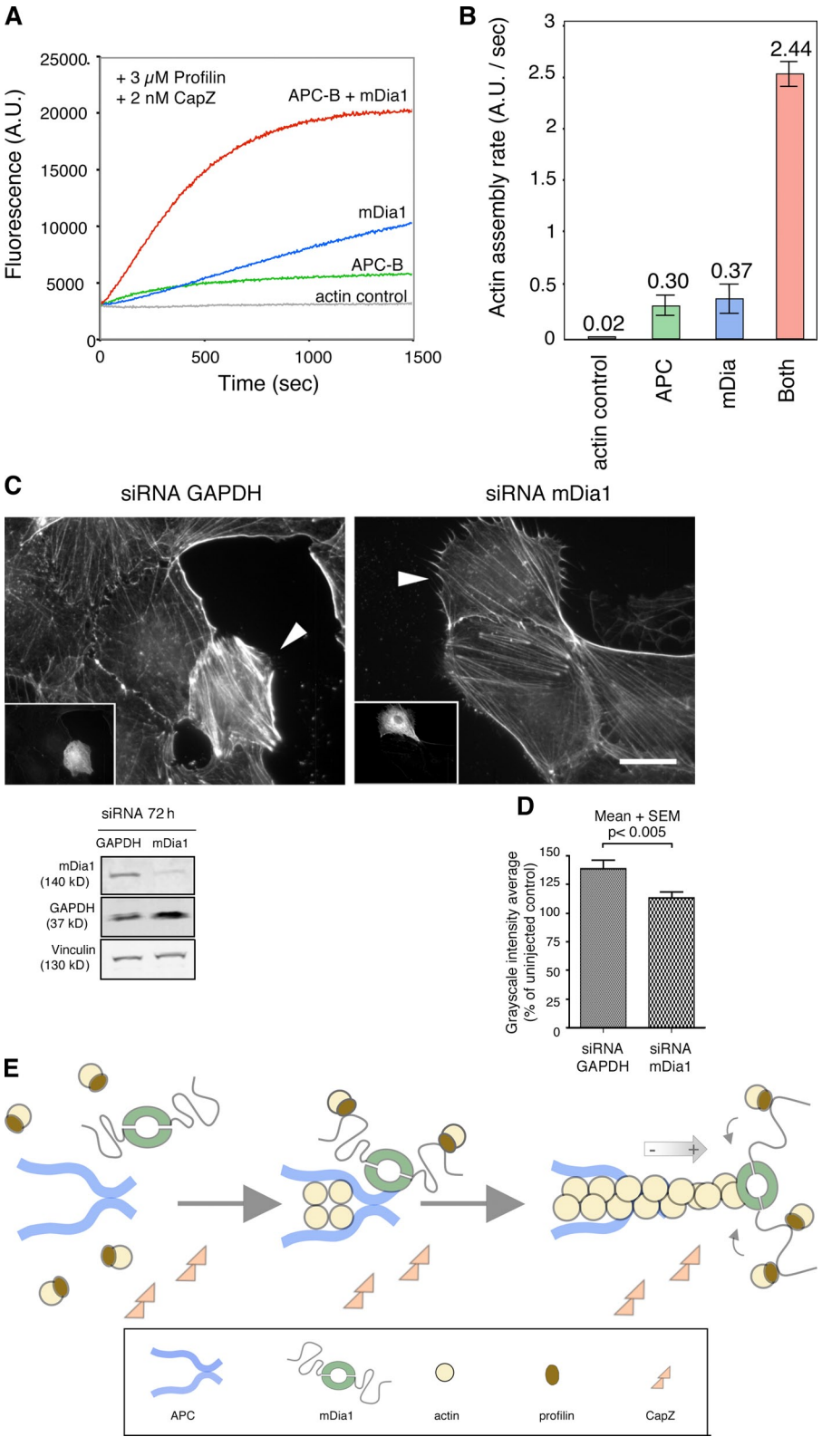

Figure 4. **mDia1 and APC-B synergize to promote actin assembly in the combined presence of profilin and capping protein.** (A) Reactions contain 2 µM actin monomers (5% pyrene labeled), 3 µM profilin, 2 nM CapZ, with or without 20 nM APC-B and/or 2 nM C-mDia1. (B) Quantification of elongation rates from the slopes of curves as in A. Rates are averages for reactions performed in triplicate in each of three separate experiments, where error bars represent standard error (n = 3). (C) Rhodamine-phalloidin staining of GAPDH or mDia1-depleted cells microinjected with EGFP-APC-B plasmid. Arrowheads point to injected cells. Insets show GFP signal for the same area. Bar, 10 µm. Right panel is an immunoblot showing expression levels 72 h after siRNA transfection for GAPDH and mDia1, with vinculin as a loading control. (D) Quantification of F-actin levels induced by EGFP-APC-B in GAPDH or mDia1-depleted cells (n > 40). (E) Model for synergy between APC and mDia1 in promoting actin assembly, where APC efficiently seeds polymer formation by recruiting actin monomers from a pool of profilin-actin to form a prenucleation complex. The barbed end of the seed is captured by the FH2 domain of mDia1, which processively moves with the growing barbed end, protecting it from capping proteins while accelerating elongation through FH1–profilin–actin interactions.

that loss of the C-terminal activities of APC may contribute to tumor progression (Samowitz et al., 1999). Indeed, one of the earliest defects observed in the intestinal epithelium of APC truncation mutant mice lacking the C terminus is aberrant cell architecture and cell migration (Oshima et al., 1997; Sansom et al., 2004). Further, the C terminus of APC is sufficient to direct localization to the actin-rich cell cortex and microtubule plus ends (Rosin-Arbesfeld et al., 2001). The C terminus of APC, which includes the Basic domain, is also indispensable for directional cell motility and normal protrusive activity in cultured cells (Kroboth et al., 2007). These observations have suggested that activities inherent to the C terminus of APC make fundamental

contributions to microtubule- and actin-based cell motility, leaving open the possibility that loss of such activities contributes to tumor progression. Future work that considers APC as a nucleator of actin assembly and a functionally synergizing binding partner of formins may help shed new light on how APC suppresses tumor formation.

Materials and methods

Plasmid construction

For expression of GFP-APC-B, GFP-APC-B-ΔN4, and GFP-APC-B-ΔN5 in NIH3T3 cells, coding sequences were PCR amplified from cDNA and subcloned into HindIII–BamHI sites of pEGFP-C3 (Takara Bio Inc.). For expression and purification of C-mDia1 (residues 549–1255) from yeast, the designated coding sequences were PCR amplified from cDNA and subcloned into pBG564 (URA3, 2μ, *GAL1/10* promoter). APC-B and APC-C polypeptides were expressed in *Escherichia coli* using plasmids described previously (Moseley et al., 2007). To generate nested deletions in APC-B (Fig. 3 A), sequences were PCR amplified from a template plasmid and subcloned into EcoRI–NotI sites of the same vector. All plasmids were verified by DNA sequencing.

Cell culture and microinjection

NIH3T3 cells were grown in DME and 10% calf serum as described previously (Palazzo et al., 2001). For microinjection experiments, confluent monolayers of NIH3T3 cells were grown on acid-washed coverslips and serum starved for 48 h in DME plus 10 mM Hepes, pH 7.4. Cells were wounded 30 min before being microinjected in their nuclei as described previously (Palazzo et al., 2001) using 135 μg/ml of plasmid DNA diluted in ddH_2O, and allowed to express for 3 h before fixation.

siRNA depletion

NIH3T3 cells were transfected with siRNA to silence GAPDH (5′-AAAGUUGUCAUGGAUGACCTT-3′) or mDia1 (5′-AAGGUGAAGGAGGACCGCUUU-3′) by using Lipofectamine RNAiMAX (Invitrogen) in accordance with the manufacturer's protocol. Protein levels were analyzed 72 h after transfection by immunoblotting with antibodies against GAPDH (rabbit 1:500; Santa Cruz Biotechnology, Inc.), mDia1 (mouse 1:500; BD), and vinculin (mouse 1:1,000; Sigma-Aldrich). For microinjection analysis, 24 h after transfection cells were serum starved for 48 h and injected with EGFP-APC-B cDNA, fixed, and processed for immunofluorescence as described below.

Epifluorescence microscopy and imaging analysis

Cells were fixed in 4% PFA in PBS for 15 min and permeabilized with 0.5% Triton X-100 in PBS for 5 min. Rhodamine-phalloidin (1:200; Invitrogen) was used to detect F-actin. Cells were observed on a microscope (Optiphot; Nikon) using a 60x PlanApo objective (1.4 NA) and filter cubes optimized for GFP and rhodamine fluorescence. Images were captured with a CCD camera (MicroMAx; KAF 1400 chip; Kodak) running MetaMorph software (MDS Analytical Technologies). To quantify cellular F-actin staining, one region was drawn around the perimeter of the injected cell and another around the perimeter of a noninjected control cell in the same frame. Gray intensity average values were measured by MetaMorph software and their ratio calculated after background subtraction using Excel (Microsoft). Statistical analysis of data was performed using Prism 4 (GraphPad Software, Inc.). All images shown in figures were processed and assembled using Photoshop (Adobe).

Protein purification

To circumvent issues of APC susceptibility to proteolytic degradation during its purification, we used separate affinity tags on either end (N-terminal GST, C-terminal 6His) and isolated APC-B and APC-C polypeptides from *E. coli* devoid of degraded products (Fig. 1 A). These proteins were purified sequentially on Ni-NTA (QIAGEN) and glutathione-agarose beads (GE Healthcare) as described previously (Moseley et al., 2007). Glutathione-eluted proteins were purified further by gel filtration on a Superose 6 column (GE Healthcare) equilibrated in 20 mM Tris-HCl, 600 mM KCl, 0.5 mM DTT, and 5% glycerol, pH 8.0. Peak fractions were pooled, exchanged into storage buffer (same as above except with 300 mM KCl), aliquoted, snap-frozen in liquid N_2, and stored at −80°C. MBP-APC-C polypeptide was purified on amylose resin (New England Biolabs, Inc.), then by gel filtration as above. C-mDia1 was purified as described previously (Moseley et al., 2006). Human profilin and chicken CapZ were expressed in *E. coli* and purified as described previously (Soeno et al., 1998; Moseley et al., 2004). Rabbit skeletal muscle actin (RMA) was purified as described previously (Spudich and Watt, 1971) and gel filtered. For fluorometric assays, RMA was labeled with pyrenyl iodoacetamide (Cooper et al., 1983), and for TIRF analysis RMA was labeled on lysines with Alexa 532–succinimidyl-ester (Kellogg et al., 1988). Unlabeled tubulin was purified from bovine brain as described previously (Goode et al., 1999).

Actin assembly and disassembly assays

Gel-filtered Ca^{2+}-ATP actin monomers (5% pyrene labeled) in G-buffer (3 mM Tris, 0.1 mM $CaCl_2$, 0.2 mM DTT, and 0.2 mM ATP, pH 7.5) were converted to Mg^{2+}-ATP actin by adding 0.1 vol of 10 mM EGTA and 1 mM $MgCl_2$ and incubating for 2 min on ice. The actin was mixed with other proteins or control buffer, and polymerization was initiated by addition of 0.1 vol of 10x initiation mix (500 mM KCl, 20 mM $MgCl_2$, 10 mM EGTA, 2 mM ATP, and 200 mM Tris-HCl, pH 8.0). Pyrene fluorescence was monitored at excitation 365 nm and emission 407 nm in a fluorescence spectrophotometer (Photon Technology International). For seeded filament elongation assays (Fig. 1 I), preassembled F-actin (0.66 μM in the final reaction) was sheared in the presence or absence of 20 nM APC-B and/or 100 nM CapZ, then mixed with 2 μM G-actin (5% pyrene labeled) and monitored for polymerization. For actin disassembly assays (Fig. 1 G), preassembled F-actin (2 μM final; 5% pyrene labeled) was mixed with Cof1 (125 or 300 nM), 50 nM APC-B, or control buffer, then Vitamin-D binding protein was added to initiate net disassembly.

Sedimentation velocity analyses and analytical gel filtration

Sedimentation coefficients (S value) of polypeptides were determined as described previously using sucrose gradient fractionation (Balcer et al., 2003). 10–50 μg of purified polypeptide was loaded on a 12.6-ml sucrose gradient (3–30%) and centrifuged for 18 h at 4°C in a rotor (SW40 Ti; Beckman Coulter) at 30,000 rpm. 400 μl fractions were harvested, and samples of each fraction were analyzed by immunoblotting. For gel filtration analysis, polypeptides were loaded on a Superose 6 column (AP Biotechnology). Elution peaks were monitored by absorbance at 280 nm and verified by immunoblotting column fractions. Size standards in both analyses were: aldolase (158 kD), albumin (67 kD), focal adhesion kinase FERM fragment (46 kD), and chymotrypsinogen A (25 kD). Native molecular weight was calculated from the sedimentation coefficient and Stokes radius as described previously (Schuyler and Pellman, 2002).

G-actin–binding analysis

For native PAGE assays, 3 μl (0.5 μg) of Ca-ATP–G-actin preincubated with latrunculin B in G-buffer was incubated for 10 min with or without 3 μl APC-B (0.5 μg; wild type or truncated) in storage buffer described above. Then 3 μl of 3x loading buffer (75 mM Tris, 0.6 M glycine, 0.6 mM ATP, $CaCl_2$, 0.6 mM DTT, and 15% glycerol) was added before loading on native gel. Final reactions had 100 mM KCl and were fractionated on 7.5% native gels or 2.5% gels supplemented with 0.5% agarose as described previously (Moseley et al., 2004). For fluorescence-based assays, 100 nM Ca-ATP–G-actin (100% pyrene labeled) was preincubated for 5 min with 100 nM latrunculin B in G-buffer. Then 55 μl of this mixture was added to 5 μl of APC-B in storage buffer (0–75 nM final; see Fig. 2 F), and fluorescence levels were measured when reactions reached steady state.

Electron microscopy

G-actin (1.8 μM) was mixed with APC-C (50 nM) or control buffer, and actin polymerization was initiated by addition of initiation mix. After 30 s, samples were adsorbed onto carbon-coated Cu grids for 50 s and stained with 2% (wt/vol) uranyl acetate. Images were collected on an electron microscope (Morgagni 268; FEI) operating at 80 kV.

TIRF microscopy

TIRF microscopy was performed as described previously with minor modifications (Kovar et al., 2006). Glass flow cells were incubated with 100 nM *N*-ethylmaleimide (NEM)–myosin for 2–5 min, washed extensively with 1% BSA, and equilibrated with TIRF buffer (10 mM imidazole, pH 7.0, 50 mM KCl, 1 mM $MgCl_2$, 1 mM EGTA, 50 mM DTT, 0.2 mM ATP, 50 nM $CaCl_2$, 15 mM glucose, 20 μg/ml catalase, 100 μg/ml glucose oxidase, and 0.5% methylcellulose). 4 μl of Mg-ATP actin monomers (30% Alexa 532 labeled) was mixed with 6 μl of proteins (profilin, APC-B and/or C-mDia1; final concentrations in figure legend) or control buffer, and then added to 10 μl of 2x TIRF buffer. Final reactions contained 1 μM actin. Samples of reactions were transferred to a flow cell, and image acquisition was initiated within 2–5 min. Images were captured on a microscope (Eclipse GE2000-S; Nikon) equipped with an iXon EM-CCD camera (Andor Technology PLC)

and 100x PlanApo 1.40 NA objective with prism-based TIRF illumination from a 473-nm laser. Images were collected at 5-s intervals for 0.5-s exposure times. Data were processed using ImageJ (NIH, Bethesda, MD) and IDL version 6.3 (ITT Visual Information Solution).

Online supplemental material

Fig. S1 shows an alignment of APC-B sequences from multiple organisms. Fig. S2 shows a side-by-side activity comparison of APC-B and APC-C actin nucleation activities, and binding of APC-B to G-actin in 50 mM KCl. Fig. S3 shows the actin nucleation activities, G-actin–binding interactions, and microtubule-binding interactions of truncated APC-B polypeptides. Videos 1–3 show TIRF movies of actin filament assembly quantified in Fig. 2 D. Online supplemental material is available at http://www.jcb.org/cgi/content/full/jcb.201001016/DC1.

We thank R. Dominguez for examining the APC-B sequence for potential WH2 domains and C. Gould for assistance in the sedimentation velocity experiments. A.M. Deaconescu is an HHMI fellow of the Damon Runyon Cancer Research Foundation.

This work was supported by National Institutes of Health research grants to G.G. Gundersen (GM62939) and B.L. Goode (GM63691 and GM083137).

Submitted: 5 January 2010
Accepted: 28 May 2010

References

Ahuja, R., R. Pinyol, N. Reichenbach, L. Custer, J. Klingensmith, M.M. Kessels, and B. Qualmann. 2007. Cordon-bleu is an actin nucleation factor and controls neuronal morphology. *Cell.* 131:337–350. doi:10.1016/j.cell.2007.08.030

Balcer, H.I., A.L. Goodman, A.A. Rodal, E. Smith, J. Kugler, J.E. Heuser, and B.L. Goode. 2003. Coordinated regulation of actin filament turnover by a high-molecular-weight Srv2/CAP complex, cofilin, profilin, and Aip1. *Curr. Biol.* 13:2159–2169. doi:10.1016/j.cub.2003.11.051

Bosch, M., K.H. Le, B. Bugyi, J.J. Correia, L. Renault, and M.F. Carlier. 2007. Analysis of the function of Spire in actin assembly and its synergy with formin and profilin. *Mol. Cell.* 28:555–568. doi:10.1016/j.molcel.2007.09.018

Carramusa, L., C. Ballestrem, Y. Zilberman, and A.D. Bershadsky. 2007. Mammalian diaphanous-related formin Dia1 controls the organization of E-cadherin-mediated cell-cell junctions. *J. Cell Sci.* 120:3870–3882. doi:10.1242/jcs.014365

Chereau, D., M. Boczkowska, A. Skwarek-Maruszewska, I. Fujiwara, D.B. Hayes, G. Rebowski, P. Lappalainen, T.D. Pollard, and R. Dominguez. 2008. Leiomodin is an actin filament nucleator in muscle cells. *Science.* 320:239–243. doi:10.1126/science.1155313

Chesarone, M.A., and B.L. Goode. 2009. Actin nucleation and elongation factors: mechanisms and interplay. *Curr. Opin. Cell Biol.* 21:28–37. doi:10.1016/j.ceb.2008.12.001

Cooper, J.A., S.B. Walker, and T.D. Pollard. 1983. Pyrene actin: documentation of the validity of a sensitive assay for actin polymerization. *J. Muscle Res. Cell Motil.* 4:253–262. doi:10.1007/BF00712034

Drubin, D.G., and W.J. Nelson. 1996. Origins of cell polarity. *Cell.* 84:335–344. doi:10.1016/S0092-8674(00)81278-7

Goode, B.L., J.J. Wong, A.C. Butty, M. Peter, A.L. McCormack, J.R. Yates, D.G. Drubin, and G. Barnes. 1999. Coronin promotes the rapid assembly and cross-linking of actin filaments and may link the actin and microtubule cytoskeletons in yeast. *J. Cell Biol.* 144:83–98. doi:10.1083/jcb.144.1.83

Joslyn, G., D.S. Richardson, R. White, and T. Alber. 1993. Dimer formation by an N-terminal coiled coil in the APC protein. *Proc. Natl. Acad. Sci. USA.* 90:11109–11113. doi:10.1073/pnas.90.23.11109

Kawasaki, Y., T. Senda, T. Ishidate, R. Koyama, T. Morishita, Y. Iwayama, O. Higuchi, and T. Akiyama. 2000. Asef, a link between the tumor suppressor APC and G-protein signaling. *Science.* 289:1194–1197. doi:10.1126/science.289.5482.1194

Kelleher, J.F., S.J. Atkinson, and T.D. Pollard. 1995. Sequences, structural models, and cellular localization of the actin-related proteins Arp2 and Arp3 from Acanthamoeba. *J. Cell Biol.* 131:385–397. doi:10.1083/jcb.131.2.385

Kellogg, D.R., T.J. Mitchison, and B.M. Alberts. 1988. Behaviour of microtubules and actin filaments in living *Drosophila* embryos. *Development.* 103:675–686.

Kita, K., T. Wittmann, I.S. Näthke, and C.M. Waterman-Storer. 2006. Adenomatous polyposis coli on microtubule plus ends in cell extensions can promote microtubule net growth with or without EB1. *Mol. Biol. Cell.* 17:2331–2345. doi:10.1091/mbc.E05-06-0498

Kovar, D.R., and T.D. Pollard. 2004. Insertional assembly of actin filament barbed ends in association with formins produces piconewton forces. *Proc. Natl. Acad. Sci. USA.* 101:14725–14730. doi:10.1073/pnas.0405902101

Kovar, D.R., E.S. Harris, R. Mahaffy, H.N. Higgs, and T.D. Pollard. 2006. Control of the assembly of ATP- and ADP-actin by formins and profilin. *Cell.* 124:423–435. doi:10.1016/j.cell.2005.11.038

Kroboth, K., I.P. Newton, K. Kita, D. Dikovskaya, J. Zumbrunn, C.M. Waterman-Storer, and I.S. Näthke. 2007. Lack of adenomatous polyposis coli protein correlates with a decrease in cell migration and overall changes in microtubule stability. *Mol. Biol. Cell.* 18:910–918. doi:10.1091/mbc.E06-03-0179

Li, R., and G.G. Gundersen. 2008. Beyond polymer polarity: how the cytoskeleton builds a polarized cell. *Nat. Rev. Mol. Cell Biol.* 9:860–873. doi:10.1038/nrm2522

McCartney, B.M., and I.S. Näthke. 2008. Cell regulation by the Apc protein Apc as master regulator of epithelia. *Curr. Opin. Cell Biol.* 20:186–193. doi:10.1016/j.ceb.2008.02.001

Moseley, J.B., I. Sagot, A.L. Manning, Y. Xu, M.J. Eck, D. Pellman, and B.L. Goode. 2004. A conserved mechanism for Bni1- and mDia1-induced actin assembly and dual regulation of Bni1 by Bud6 and profilin. *Mol. Biol. Cell.* 15:896–907. doi:10.1091/mbc.E03-08-0621

Moseley, J.B., S. Maiti, and B.L. Goode. 2006. Formin proteins: purification and measurement of effects on actin assembly. *Methods Enzymol.* 406:215–234. doi:10.1016/S0076-6879(06)06016-2

Moseley, J.B., F. Bartolini, K. Okada, Y. Wen, G.G. Gundersen, and B.L. Goode. 2007. Regulated binding of adenomatous polyposis coli protein to actin. *J. Biol. Chem.* 282:12661–12668. doi:10.1074/jbc.M610615200

Munemitsu, S., B. Souza, O. Müller, I. Albert, B. Rubinfeld, and P. Polakis. 1994. The APC gene product associates with microtubules *in vivo* and promotes their assembly *in vitro. Cancer Res.* 54:3676–3681.

Oshima, H., M. Oshima, M. Kobayashi, M. Tsutsumi, and M.M. Taketo. 1997. Morphological and molecular processes of polyp formation in Apc(delta716) knockout mice. *Cancer Res.* 57:1644–1649.

Palazzo, A.F., T.A. Cook, A.S. Alberts, and G.G. Gundersen. 2001. mDia mediates Rho-regulated formation and orientation of stable microtubules. *Nat. Cell Biol.* 3:723–729. doi:10.1038/35087035

Pring, M., M. Evangelista, C. Boone, C. Yang, and S.H. Zigmond. 2003. Mechanism of formin-induced nucleation of actin filaments. *Biochemistry.* 42:486–496. doi:10.1021/bi026520j

Quinlan, M.E., J.E. Heuser, E. Kerkhoff, and R.D. Mullins. 2005. *Drosophila* Spire is an actin nucleation factor. *Nature.* 433:382–388. doi:10.1038/nature03241

Quinlan, M.E., S. Hilgert, A. Bedrossian, R.D. Mullins, and E. Kerkhoff. 2007. Regulatory interactions between two actin nucleators, Spire and Cappuccino. *J. Cell Biol.* 179:117–128. doi:10.1083/jcb.200706196

Romero, S., C. Le Clainche, D. Didry, C. Egile, D. Pantaloni, and M.F. Carlier. 2004. Formin is a processive motor that requires profilin to accelerate actin assembly and associated ATP hydrolysis. *Cell.* 119:419–429. doi:10.1016/j.cell.2004.09.039

Rosin-Arbesfeld, R., G. Ihrke, and M. Bienz. 2001. Actin-dependent membrane association of the APC tumour suppressor in polarized mammalian epithelial cells. *EMBO J.* 20:5929–5939. doi:10.1093/emboj/20.21.5929

Samowitz, W.S., M.D. Powers, L.N. Spirio, F. Nollet, F. van Roy, and M.L. Slattery. 1999. Beta-catenin mutations are more frequent in small colorectal adenomas than in larger adenomas and invasive carcinomas. *Cancer Res.* 59:1442–1444.

Sansom, O.J., K.R. Reed, A.J. Hayes, H. Ireland, H. Brinkmann, I.P. Newton, E. Batlle, P. Simon-Assmann, H. Clevers, I.S. Nathke, et al. 2004. Loss of Apc in vivo immediately perturbs Wnt signaling, differentiation, and migration. *Genes Dev.* 18:1385–1390. doi:10.1101/gad.287404

Schuyler, S.C., and D. Pellman. 2002. Analysis of the size and shape of protein complexes from yeast. *Methods Enzymol.* 351:150–168. doi:10.1016/S0076-6879(02)51845-0

Soeno, Y., H. Abe, S. Kimura, K. Maruyama, and T. Obinata. 1998. Generation of functional beta-actinin (CapZ) in an *E. coli* expression system. *J. Muscle Res. Cell Motil.* 19:639–646. doi:10.1023/A:1005329114263

Spudich, J.A., and S. Watt. 1971. The regulation of rabbit skeletal muscle contraction. I. Biochemical studies of the interaction of the tropomyosin-troponin complex with actin and the proteolytic fragments of myosin. *J. Biol. Chem.* 246:4866–4871.

Su, L.K., M. Burrell, D.E. Hill, J. Gyuris, R. Brent, R. Wiltshire, J. Trent, B. Vogelstein, and K.W. Kinzler. 1995. APC binds to the novel protein EB1. *Cancer Res.* 55:2972–2977.

Watanabe, N., P. Madaule, T. Reid, T. Ishizaki, G. Watanabe, A. Kakizuka, Y. Saito, K. Nakao, B.M. Jockusch, and S. Narumiya. 1997. p140mDia, a mammalian homolog of *Drosophila* diaphanous, is a target protein for Rho small GTPase and is a ligand for profilin. *EMBO J.* 16:3044–3056. doi:10.1093/emboj/16.11.3044

Watanabe, T., S. Wang, J. Noritake, K. Sato, M. Fukata, M. Takefuji, M. Nakagawa, N. Izumi, T. Akiyama, and K. Kaibuchi. 2004. Interaction with IQGAP1 links APC to Rac1, Cdc42, and actin filaments during cell polarization and migration. *Dev. Cell.* 7:871–883. doi:10.1016/j.devcel.2004.10.017

Wen, Y., C.H. Eng, J. Schmoranzer, N. Cabrera-Poch, E.J. Morris, M. Chen, B.J. Wallar, A.S. Alberts, and G.G. Gundersen. 2004. EB1 and APC bind to mDia to stabilize microtubules downstream of Rho and promote cell migration. *Nat. Cell Biol.* 6:820–830. doi:10.1038/ncb1160

Zigmond, S.H., M. Evangelista, C. Boone, C. Yang, A.C. Dar, F. Sicheri, J. Forkey, and M. Pring. 2003. Formin leaky cap allows elongation in the presence of tight capping proteins. *Curr. Biol.* 13:1820–1823. doi:10.1016/j.cub.2003.09.057

Zuchero, J.B., A.S. Coutts, M.E. Quinlan, N.B. Thangue, and R.D. Mullins. 2009. p53-cofactor JMY is a multifunctional actin nucleation factor. *Nat. Cell Biol.* 11:451–459. doi:10.1038/ncb1852